ACS OMEGA

http://pubs.acs.org/journal/acsodf

Article

Adsorption Properties of Pt_n (n = 1−3) Cluster-Doped SnS_2 and $MoTe_2$ toward Vehicle Emissions: CO, CO_2, and NO

Yanshan Zhang, Shoucheng Yan,* and Yawei Zhu

Cite This: *ACS Omega* 2023, 8, 29746−29757

Read Online

ACCESS | Metrics & More | Article Recommendations

ABSTRACT: The interaction mechanism between CO, CO_2, and NO gas molecules and Pt_n-SnS_2 (n = 1−3) and Pt_n-$MoTe_2$ (n = 1−3) is analyzed based on density functional theory calculations. For Pt_2-SnS_2, the structure of Pt_2-SnS_2 is deformed during CO_2 adsorption. For Pt_3-SnS_2, its structure is also significantly deformed when the gas is adsorbed. Pt_2-SnS_2 is not suitable for the detection and adsorption of CO_2 gas, while Pt_3-SnS_2 is not suitable for the detection and adsorption of these three gases. According to the density of states and molecular orbital analysis, the conductivity of the adsorption system of Pt-SnS_2 remains almost unchanged after the adsorption of CO, so Pt-SnS_2 is not suitable for the detection of CO gases. The adsorption of gases on intrinsic $MoTe_2$ is a weakly interacting physical adsorption. Doping with one to three Pt atoms all resulted in different degrees of enhancement of the adsorption capacity of the substrates for these three target gases. However, for Pt_2-$MoTe_2$ and Pt_3-$MoTe_2$, the structure of these two materials undergoes significant deformation upon NO adsorption. In addition, the interaction between Pt_3-$MoTe_2$ and CO_2 is weak, and the conductivity of this system is almost unaffected by CO_2 adsorption. In addition, all other constructions are suitable for the detection of the corresponding gases. This paper provides a theoretical basis for the development of gas sensors for the detection of automotive and industrial emission gases.

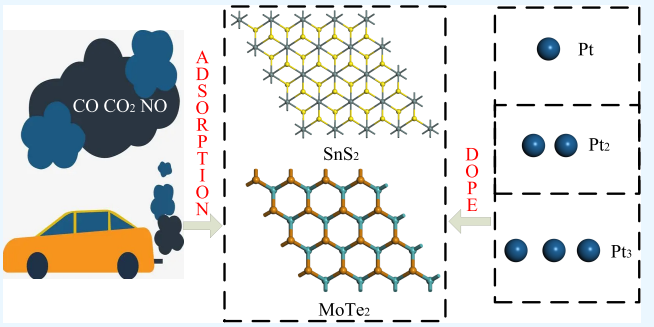

1. INTRODUCTION

With the continuous development of the automotive industry, the phenomenon of vehicle noxious emissions is becoming more and more serious, which causes environmental damage and threatens human life and health.[1] Among the gas emissions, CO_2 has been causing the greenhouse effect, leading to global warming. CO is a toxic and harmful gas mainly produced by incomplete combustion, which can cause death at high concentrations. Nitrogen oxides are also a major category of vehicle emissions, of which 95% are NO.[2] CO and NO emissions can cause acid rain and smog and damage the ozone layer.[3,4] Problems such as neurological and cardiovascular diseases caused by exposure to these pollutants have attracted a great deal of attention.[5] To reduce environmental problems raised by vehicle emissions, it is necessary to develop an effective detection method for these noxious vehicle emission gases.

Two-dimensional nanomaterials with a large specific surface area and high chemical activity are considered as ideal gas-sensitive materials and have received much attention in the field of gas sensing.[6−12] Monolayer SnS_2 and $MoTe_2$ are two typical members of them. Transition metal dichalcogenides (TMDCs) have a wide range of applications in electronic devices. The D-dependent E_g (D) of two-dimensional TMDCs is investigated free of adjustable parameters with the band-gap thermodynamic study.[13] Based on a band-gap thermodynamic study, the composition and layer-dependent band-gap energy of two-dimensional TMDC alloys is modeled without any adjustable parameters.[14] There are also studies related to catalysis, and using density functional theory (DFT) calculations, intrinsic defects in the basal plane of WS_2, including vacancy defects and antisite defects, were created with high-loading TM active sites for boosting nitrogen reduction reaction.[15] Antisite defects of MoS_2 and WS_2 and intrinsic atomic defects of MoS_2 and WS_2 with a transition metal atom substituting a S_2 column were investigated for CO reduction reaction by DFT calculations.[16] In recent years, various modification methods based on monolayer SnS_2 and monolayer $MoTe_2$ have been investigated. Chen et al. studied the gas-sensitive properties of CuO- and NiO-modified SnS_2 surfaces on C_2H_4, CH_4, H_2, and H_2O and found that they have good adsorption effects on C_2H_4.[17] Peng et al. studied the gas-

Received: June 12, 2023
Accepted: July 25, 2023
Published: August 2, 2023

© 2023 The Authors. Published by American Chemical Society

https://doi.org/10.1021/acsomega.3c04158
ACS Omega 2023, 8, 29746−29757

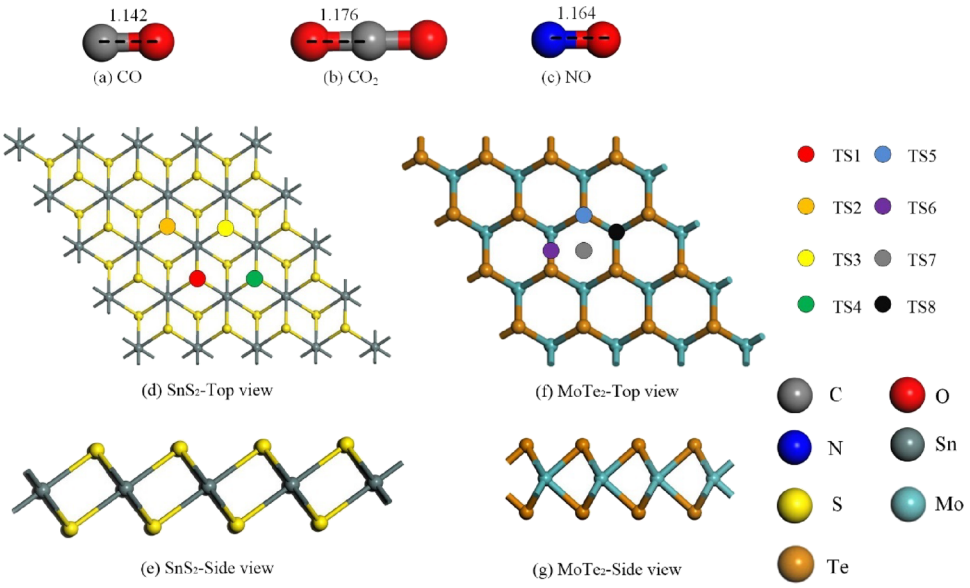

Figure 1. (a–g) Optimized structures of CO, CO_2, NO, SnS_2, and $MoTe_2$ and various doping sites ranging from TS1 to TS8. The distance unit is Å.

sensitive properties of Ru-cluster-modified SnS_2 surfaces on dissolved gases in transformer oil and found that Ru_3-SnS_2 has great potential as a gas scavenger for the removal of dissolved CO, C_2H_2, and C_2H_4 from transformer oil.[18] Shi et al. found that the adsorption performance of Pd-, Ni-, and Pt-modified $MoTe_2$ on NH_3 and SO_2 was significantly improved.[19] Liu et al. studied the adsorption performance of CuO-, Ag_2O-, and In_2O_3-modified $MoTe_2$ on NH_3, NO, and C_2H_2 and found that CuO-$MoTe_2$ can be used as a promising recyclable heating-type sensor for NH_3 and C_2H_2, and Ag_2O-$MoTe_2$ can be used as a reliable adsorbent for C_2H_2 and NO at room temperature.[20] The adsorption characteristics of Pt-$MoTe_2$ for dissolved gases in transformer oil were studied by Jiang et al.[21] The adsorption characteristics of Pt-cluster SnS_2 for SF_6 characteristic decomposition gases were studied by Chen et al.[22] Inspired by the related studies, this paper proposes the application of Pt_n-SnS_2 and Pt_n-$MoTe_2$ for the detection of toxic and hazardous vehicle emission gases (CO, CO_2, and NO).

In this study, the interaction mechanism between CO, CO_2, NO gas molecules and Pt_n-SnS_2 (n = 1–3), Pt_n-$MoTe_2$ (n = 1–3) is analyzed from the perspective of adsorption structure, energy band structure, density of states (DOS), and molecular orbitals based on DFT. This paper provides a theoretical basis for the development of gas sensors for the detection of vehicle emission gases.

2. COMPUTATIONAL DETAILS AND METHODS

All calculations were performed based on the DFT applying the Dmol^3 module.[23,24] The lattice parameters of the constructed supercell of SnS_2 and $MoTe_2$ single layers were a = 14.7997 Å, b = 14.7997 Å, and c = 32.9557 Å and a = 14.2348 Å, b = 14.2348 Å, and c = 33.6193 Å, respectively. The vacuum layer was set to 20 Å to avoid the interaction between the adjacent layers.[25] The Perdew–Burke–Ernzerhof function in the generalized gradient approximation was chosen to calculate the electron exchange and correlation energy.[26] The orbital electron distribution was calculated using the DFT semi-core pseudopods method. The Tkatchenko and Scheffler algorithm was used to obtain more accurate calculation results.[17,25] Meanwhile, the spin-polarization calculation was considered.[27,28] The double numerical plus polarization basis set was used.[29] The energy convergence accuracy, maximum stress, and maximum displacement were set to 1.0×10^{-5} Ha, 0.002 Ha/Å, and 0.005 Å, respectively. The self-consistent field convergence accuracy and the global orbital cutoff radius were set to 1.0×10^{-6} Ha and 5.0 Å, respectively. To reduce the calculation time, DIIS is set to 6. The K points of the band structure that are calculated using fine, empty bands are set to 12, and the separation is set to 0.015 1/Å. The Monkhorst–Pack k-point grid of 5 × 5 × 1 was used for geometric optimization and DOS analysis.[30−32] The calculation parameters of the gas molecular model are the same as those of the above substrate model, but the difference is that the Monkhorst–Pack k-point grid is fine, and no property calculation is carried out, such as the band structure, DOS, and electron density.

The binding energy (E_b) can be calculated by eq 1, where $E_{Ptn\text{-}suf}$, E_{suf}, and E_{Ptn} represent the energy of the substrate after Pt_n doping, the energy of the substrate before doping, and the energy of the Pt_n cluster, respectively. The adsorption energy (E_{ads}) of the adsorption system was calculated by eq 2, where $E_{gas/suf}$, E_{suf}, and E_{gas} represent the energy of the substrate after gas adsorption, the energy of the substrate before gas adsorption, and the energy of the gas molecule, respectively. The charge transfer (Q_t) was analyzed using Hirshfeld population analysis. $Q_t < 0$ represents the electron transfer from the surface to the gas molecule. The energy gap (E_g) of the molecular orbit is defined in eq 3, where E_{LUMO} and E_{HOMO} represent the energy of the lowest unoccupied molecular orbital (LUMO) and the highest occupied molecular orbital (HOMO), respectively.

$$E_b = E_{Ptn-suf} - E_{suf} - E_{Ptn} \quad (1)$$

$$E_{ads} = E_{gas/suf} - E_{suf} - E_{gas} \quad (2)$$

$$E_g = |E_{LUMO} - E_{HOMO}| \quad (3)$$

https://doi.org/10.1021/acsomega.3c04158
ACS Omega 2023, 8, 29746–29757

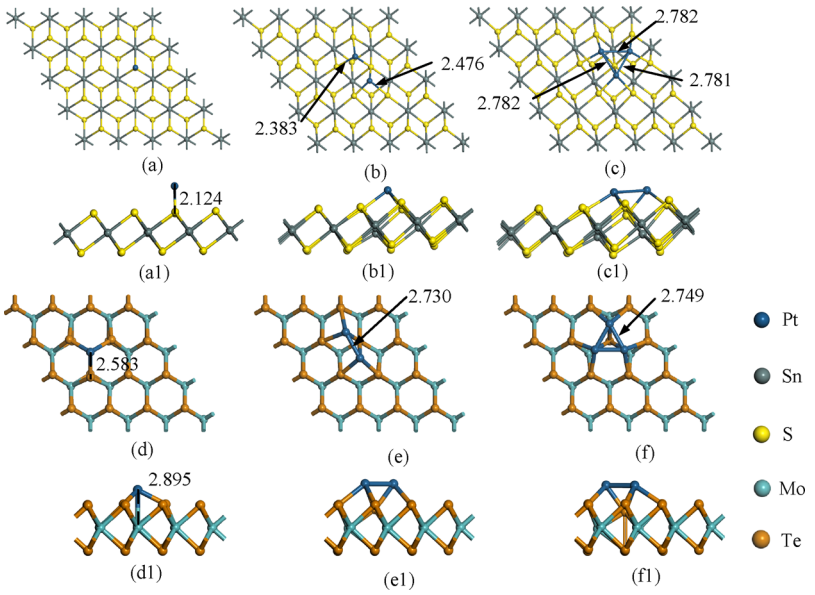

Figure 2. Optimal structures of (a, a1) Pt-SnS_2, (b, b1) Pt_2-SnS_2, (c, c1) Pt_3-SnS_2, (d, d1) Pt-$MoTe_2$, (e, e1) Pt_2-$MoTe_2$, and (f, f1) Pt_3-$MoTe_2$. (a−f) Top view. (a1−f1) Side view. The distance unit is Å.

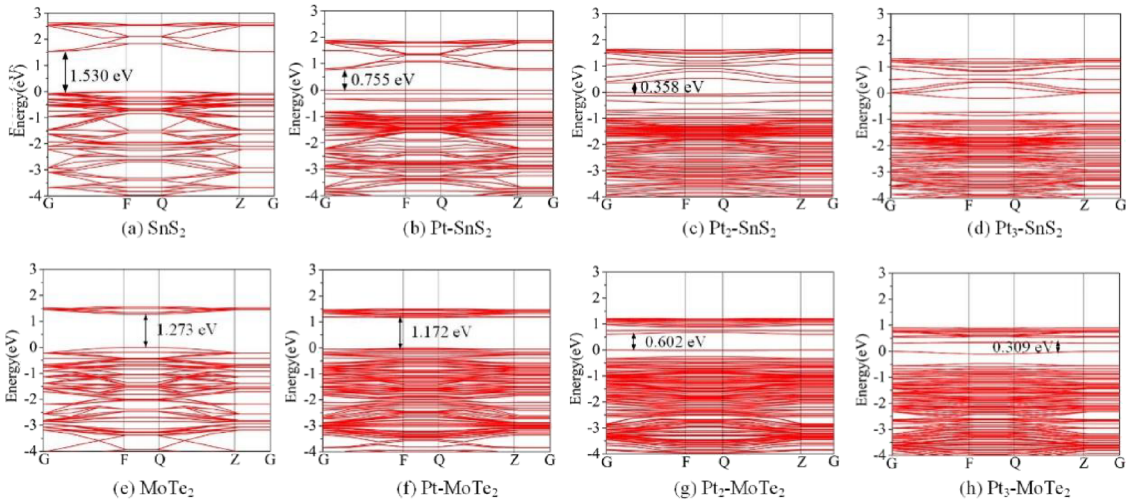

Figure 3. Band structure of (a) pristine SnS_2, (b) Pt-SnS_2, (c) Pt_2-SnS_2, (d) Pt_3-SnS_2, (e) pristine $MoTe_2$, (f) Pt-$MoTe_2$, (g) Pt_2-$MoTe_2$, and (h) Pt_3-$MoTe_2$.

3. RESULTS AND DISCUSSION

3.1. Geometric Structures of Gas Molecules, SnS_2, $MoTe_2$, Pt_n-SnS_2, and Pt_n-$MoTe_2$. The structures of the gas molecules after optimization are shown in Figure 1a−c. The bond lengths of the C−O bond in the CO molecule, the N−O bond in the NO molecule, and the C−O bond in the CO_2 molecule are very close, which are 1.142, 1.164, and 1.176 Å, respectively. At the same time, the C atom in the CO_2 molecule is located at the center of the two O atoms, and the two C−O bonds have the same length. Figure 1d−g shows the top view and side view structures of the optimized SnS_2 and $MoTe_2$. In Figure 1d,e, TS1, TS2, TS3, and TS4 are the doping sites considered for the SnS_2 monolayer. Similarly, the doping sites on $MoTe_2$ are labeled as TS5, TS6, TS7, and TS8, as shown in Figure 1f,g. To find the most stable structures for Pt-cluster (1−3) doping, various combinations of these eight sites were considered to explore the corresponding stable Pt doping structure after structural optimization.

Figure 2a−c shows the stable doping structures of single Pt atoms, double Pt atoms, and triple Pt atoms, respectively. In Figure 2a,a1, the bond length of the S-Pt bond in the Pt-SnS_2 structure is 2.214 Å, and the Pt-SnS_2 structure does not change much compared to the original SnS_2. In the Pt_2-SnS_2 structure shown in Figure 2b, the bond lengths between the two Pt atoms and the S atom at the doping position are 2.383 and 2.476 Å, respectively. In the Pt_3-SnS_2 structure shown in Figure 2c, chemical bonds are formed between the three Pt atoms, forming a stable triangle with bond lengths of 2.782, 2.782, and 2.781 Å, respectively. Also, in Figure 2b,c, the Pt atoms form chemical bonds with the surrounding S atoms, indicating a strong interaction and stable structure between the Pt atoms and the original SnS_2 surface. From Figure 2b1,c1, it can be seen that both Pt_2-SnS_2 and Pt_3-SnS_2 structures have been changed to some extent compared to the original SnS_2. Similarly, Figure 2d−f,d1−f1 shows the side and top views of Pt_n-$MoTe_2$, respectively. For Pt-$MoTe_2$, Pt is located at the TS8 site and forms Pt−Te bonds with Mo atoms on the

https://doi.org/10.1021/acsomega.3c04158
ACS Omega 2023, 8, 29746−29757

substrate surface, and the bond length of these bonds is 2.583 Å. At the same time, a Pt−Mo with a bond length of 2.895 Å is formed between the Pt atom and the Mo atom directly below. For Pt_2-$MoTe_2$, the two Pt atoms are located approximately at the TS7 site, and a Pt−Pt bond with a bond length of 2.730 Å is formed between the two atoms. Pt_3-$MoTe_2$ is similar to Pt_3-SnS_2, where three Pt atoms form a stable triangular structure with a Pt−Pt bond length of 2.749 Å.

To more clearly observe the effect of Pt doping on the gas-sensitive properties of pristine SnS_2 and $MoTe_2$, Figure 3 shows the band structure of SnS_2, $MoTe_2$, Pt_n-SnS_2, and Pt_n-$MoTe_2$. Table 1 lists the E_b and E_g parameters of SnS_2, $MoTe_2$, Pt_n-SnS_2, and Pt_n-$MoTe_2$. As can be seen from Figure 3 and Table 1, the E_g of the original SnS_2 is 1.530 eV, and after Pt atom doping, the E_g of Pt-SnS_2, Pt_2-SnS_2, and Pt_3-SnS_2 are reduced to 0.755, 0.358, and 0 eV, respectively. Accordingly, the E_b is −2.49 eV for Pt-SnS_2, −7.10 eV for Pt_2-SnS_2, and −11.50 eV for Pt_3-SnS_2. Because the impurity energy levels brought by Pt atoms are located between the valence and conduction bands of SnS_2, which makes the energy band structure of SnS_2 more continuous (especially Pt_3-SnS_2, whose E_g is 0, which metamorphoses from a semiconductor to a conductor), the conductivity is significantly enhanced. Similarly, from the data in Table 1, it can be known that the binding energies of Pt-$MoTe_2$, Pt_2-$MoTe_2$, and Pt_3-$MoTe_2$ are −3.050, −3.255, and −4.203 eV, respectively. Also in combination with Figure 3e−h, it can be observed that the corresponding E_g decrease from 1.273 to 1.172, 0.602, and 0.309 eV, respectively. In addition, the density of energy band structures becomes dense, which shows an increase in the conductivity of the doped structures. In general, the doping of Pt atoms improves the conductivity of the SnS_2 and $MoTe_2$ and has a positive effect on improving the gas-sensitive performances of SnS_2 and $MoTe_2$.

Table 1. E_b and E_g Parameters of SnS_2, $MoTe_2$, Pt_n-SnS_2, and Pt_n-$MoTe_2$

structure	E_b (eV)	E_g (eV)
SnS_2	without doping	1.530
Pt-SnS_2	−2.49	0.755
Pt_2-SnS_2	−7.10	0.358
Pt_3-SnS_2	−11.50	0
$MoTe_2$	without doping	1.273
Pt-$MoTe_2$	−3.050	1.172
Pt_2-$MoTe_2$	−3.255	0.602
Pt_3-$MoTe_2$	−4.203	0.309

3.2. Adsorption of CO, CO_2, and NO Gas Molecules on SnS_2 and $MoTe_2$. The most stable adsorption structures of the CO, CO_2, and NO gas molecules on the surfaces of SnS_2 and $MoTe_2$ are shown in Figure 4, and the corresponding calculated adsorption parameters are shown in Table 2. The E_{ads} of the SnS_2 monolayer for gas molecules are ranked as −0.152 eV (CO) < −0.154 eV (CO_2) < −0.226 eV (NO). The E_{ads} of the $MoTe_2$ monolayer for gas molecules are ranked as −0.122 eV (CO) < −0.131 eV (CO_2) < −0.160 eV (NO). It can be found that the E_{ads} of intrinsic SnS_2 and $MoTe_2$ are very small for gas molecules. It can be seen from Figure 4a−f that the geometric structure of the substrate remains basically unchanged after adsorption of gases. The adsorption distances of CO, CO_2, and NO on the SnS_2 surface are 3.577, 3.532, and 3.500 Å and on the $MoTe_2$ surface are 3.854, 3.801, and 3.377 Å, respectively. In addition, the corresponding charge transfer is −0.0211 *e*, −0.0219 *e*, 0.1672 *e*, −0.0121 *e*, −0.0266 *e*, and −0.0374 *e*, which indicates that the charge transfer between the substrate and the gas molecules is weak. From the above analysis, it is clear that the adsorption of CO, CO_2, and NO on SnS_2 and $MoTe_2$ is physical adsorption and the interaction between the gas and the substrate is weak.

Table 2. E_{ads}, Q_t, and Adsorption Distance of Gas Molecules on SnS_2 and $MoTe_2$[a]

system	adsorption distance (Å)	E_{ads} (eV)	Q_t (*e*)
CO/SnS_2	3.577	−0.152	−0.0211
CO_2/SnS_2	3.532	−0.154	−0.0219
NO/SnS_2	3.500	−0.226	0.1672
CO/$MoTe_2$	3.854	−0.122	−0.0121
CO_2/$MoTe_2$	3.801	−0.131	−0.0266
NO/$MoTe_2$	3.377	−0.160	−0.0374

[a]Adsorption distance: the shortest distance between two atoms in a gas molecule and substrate.

3.3. Adsorption Behavior of CO, CO_2, and NO Gas Molecules on Pt_n-SnS_2. To obtain the accurate optimization structure, CO, CO_2, and NO were placed on the surface of the Pt_n-SnS_2 monolayer at different angles and different distances, and the structure with the largest absolute value of E_{ads} was selected by geometric optimization to obtain the most stable adsorption structure, as shown in Figure 5. The corresponding adsorption parameters are shown in Table 3. Figure 5a−c

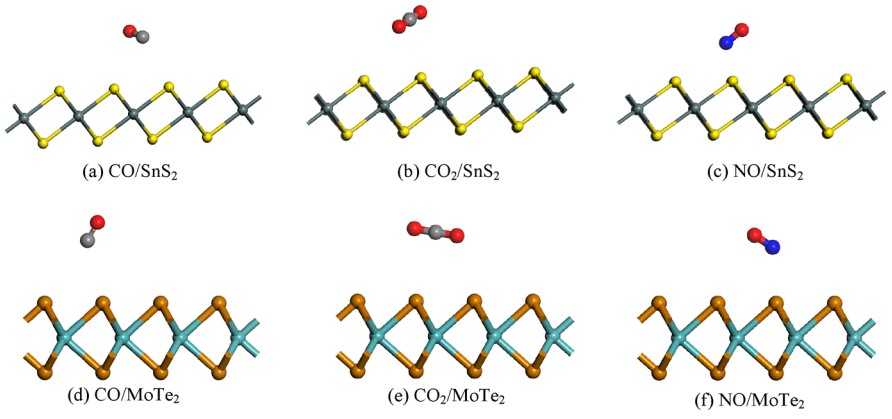

Figure 4. (a−f) CO, CO_2, and NO adsorption on SnS_2 and $MoTe_2$ surfaces. The distance unit is Å.

https://doi.org/10.1021/acsomega.3c04158
ACS Omega 2023, 8, 29746−29757

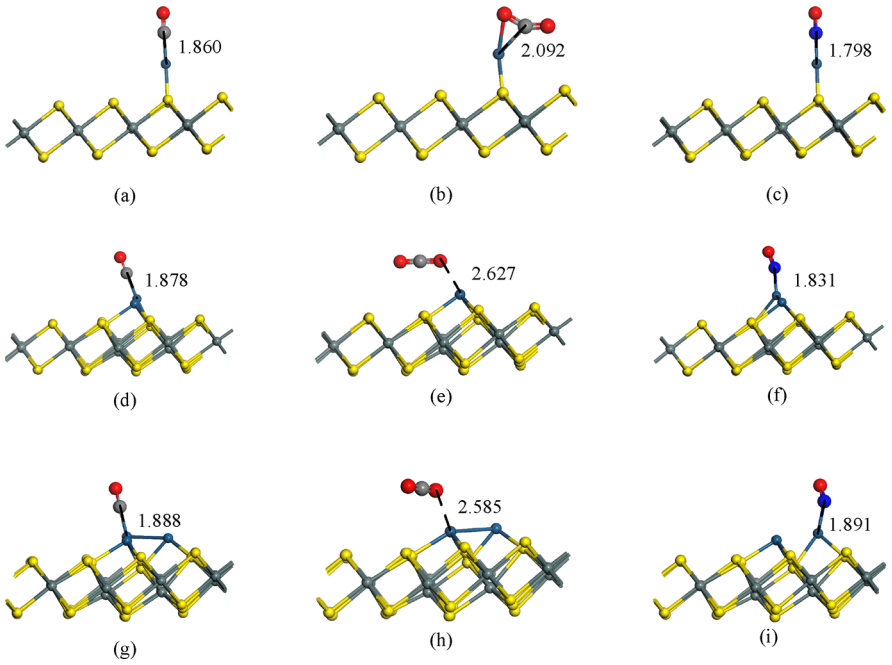

Figure 5. CO, CO_2, and NO adsorption on Pt_n-SnS_2 surfaces. (a–c) Pt-SnS_2; (d–f) Pt_2-SnS_2; (g–i) Pt_3-SnS_2. The distance unit is Å.

Table 3. E_{ads}, Q_t, and Adsorption Distance of Gas Molecules Adsorbed on Pt_n-SnS_2

structure	gas molecules	adsorption distance (Å)	E_{ads} (eV)	Q_t (e)
Pt-SnS_2	CO	1.860	−2.676	−0.0155
	CO_2	2.092	−0.783	−0.1724
	NO	1.798	−2.553	0.0691
Pt_2-SnS_2	CO	1.878	−2.106	−0.0045
	CO_2	2.627	−0.256	0.0485
	NO	1.831	−1.908	0.0052
Pt_3-SnS_2	CO	1.888	−2.040	0.0078
	CO_2	2.585	−0.253	0.0563
	NO	1.891	−1.550	0.0173

shows the most stable structures of CO, CO_2, and NO adsorbed on the Pt-SnS_2 surface. Compared with the intrinsic SnS_2, the adsorption capacity of Pt-SnS_2 is improved for CO, CO_2, and NO, and the corresponding E_{ads} are −2.676, −0.783, and −2.553 eV. At the same time, all three gas molecules form chemical bonds with the surface, and the corresponding adsorption distances are shortened to 1.860, 2.092, and 1.798 Å, respectively. From the Hirshfeld analysis, it can be seen that CO_2 receives electrons from the surface with a charge of −0.1724 e, while CO and NO transfer −0.0155 e and 0.0691 e of electrons to the surface of the substrate, respectively. The most stable structures of the gases adsorbed on the Pt_2-SnS_2 surface are shown in Figure 5d–f. From the structure diagrams, it can be found that both CO and NO form chemical bonds with Pt atoms on the surface, except for CO_2. Finally, the E_{ads} of −2.106 eV for CO, −0.256 eV for CO_2, and −1.908 eV for NO reaches the corresponding adsorption distances of 1.878, 2.627, and 1.831 Å. These adsorption data indicate that the E_{ads} of Pt_2-SnS_2 for the gas increases, and the adsorption distance decreases compared to the adsorption on the intrinsic substrate. Moreover, the charge transfer between CO, CO_2, and NO and the substrate surface is −0.0045 e, 0.0485 e, and 0.0052 e, respectively. It should be noted that the structure of Pt_2-SnS_2 changes significantly after the adsorption of CO_2, and this phenomenon is not favorable for the gas desorption process. Finally, Figure 5g–i shows the structural model of the gas molecules adsorbed by Pt_3-SnS_2. Except for CO_2, both CO and NO form chemical bonds with Pt atoms on the substrate surface. Similar to the above discussion, the E_{ads} of CO, CO_2, and NO on the Pt_3-SnS_2 surface are increased, with energies of −2.040, −0.253, and −1.550 eV, respectively, while for the adsorption distances, they are reduced to 1.888, 2.585, and 1.891 Å, respectively. CO, CO_2, and NO all provide electrons to the substrate, and the transferred charges are 0.0078 e, 0.0563 e, and 0.0173 e, respectively. In addition, it can be found that the structure of Pt_3-SnS_2 is severely distorted after adsorption of CO, CO_2, and NO, so the structure is not suitable for gas detection and adsorption. It is worth mentioning an interaction with the CO_2 bending structure within Pt-SnS_2, but it does not show a similar interaction with Pt_2-SnS_2 or Pt_3-SnS_2. According to the adsorption parameters, the adsorption distance of CO_2 on Pt-SnS_2 is the shortest, the absolute value of E_{ads} is the highest, and the charge transfer is the most intense. At the same time, C and O atoms of CO_2 form chemical bonds with Pt. These phenomena all indicate a strong interaction between CO_2 and Pt-SnS_2, which causes CO_2 to be subjected to torque force, resulting in deformation.

To further investigate the adsorption mechanism of Pt_n-SnS_2 toward different gas molecules and understand the electronic behavior more clearly, DOS analysis was performed for each adsorption system. Figure 6 shows the total density of states (TDOS) and partial density of states (PDOS) curves of all Pt_n-SnS_2-based adsorption systems. Figure 6a–c,a1–c1 shows the TDOS and PDOS of Pt-SnS_2 adsorbing CO, CO_2, and NO, respectively. The TDOS curve of the system did not change significantly after CO adsorption on the Pt-SnS_2 surface, and the conductivity of the surface system did not change significantly. The CO_2 adsorption caused the TDOS curve of the system shift to the right, which would reduce the number of electrons near the Fermi energy level, indicating a decrease in the conductivity of the adsorption system. For the adsorption of NO, the conductivity of the system decreases

https://doi.org/10.1021/acsomega.3c04158
ACS Omega 2023, 8, 29746−29757

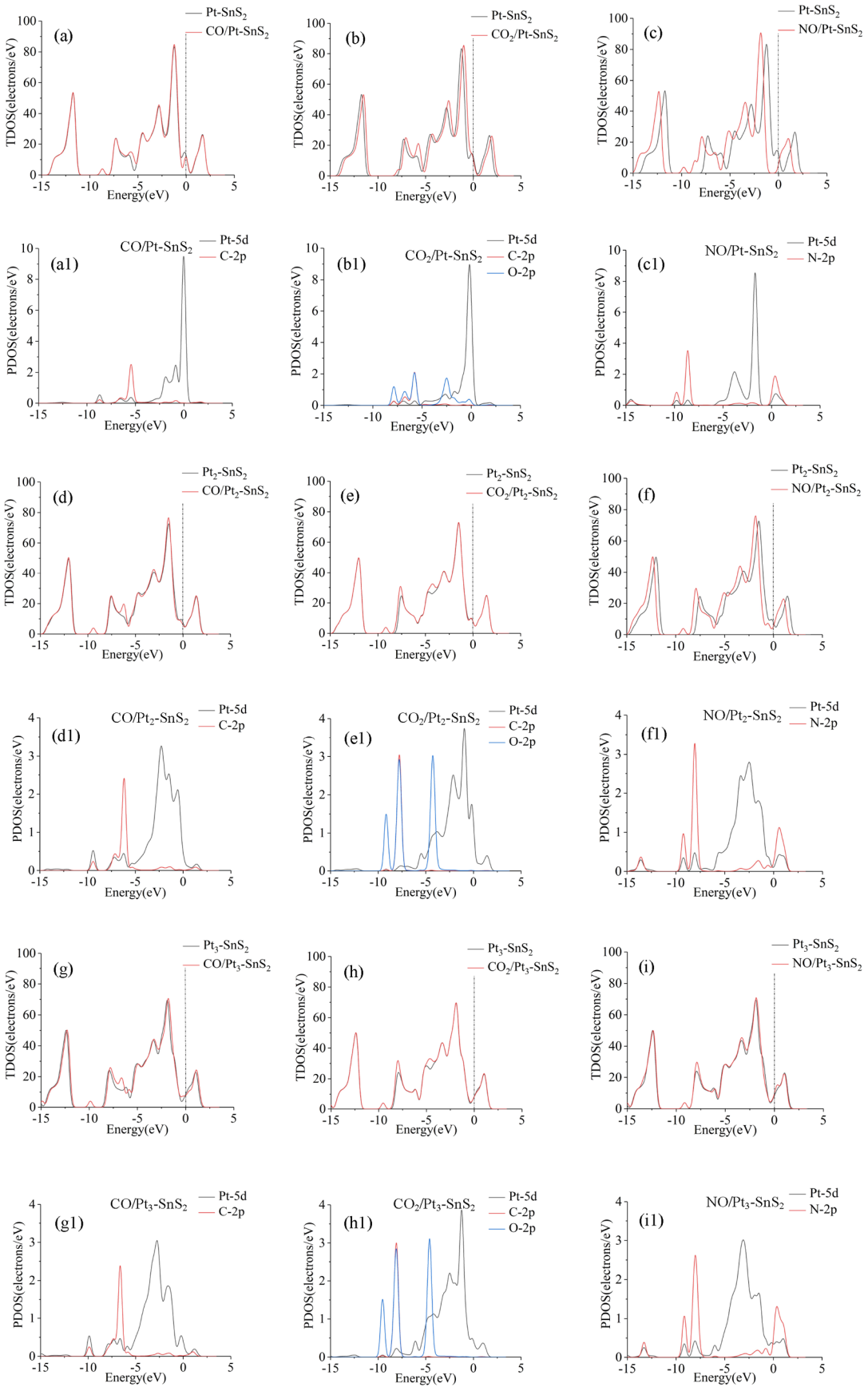

Figure 6. (a–i) TDOS and PDOS of CO, CO_2, and NO adsorption on Pt_n-SnS_2 surfaces.

https://doi.org/10.1021/acsomega.3c04158
ACS Omega 2023, 8, 29746−29757

due to the rise in the TDOS curve. The phenomenon of hybridization of atomic orbitals is responsible for the change in the TDOS curve, which can be observed by the PDOS curve. In Figure 6a1, Pt-5d undergoes orbital hybridization with C-2p of CO in the energy-level interval from −10 to −5 eV, which confirms the formation of chemical bonds between Pt and C atoms, and verifies that CO adsorption on the Pt-SnS_2 surface is chemisorption. Similarly, Figure 6b1,c1 shows that Pt-5d overlaps with C-2p and O-2p in the interval from −10 to −5 eV, respectively, and Pt-5d overlaps with N-2p in the range from −10 to −7.5 eV, indicating that a significant hybridization occurs between these orbitals, confirming the existence of Pt−C bonds and Pt−N bonds and verifying that CO_2 and NO adsorption on the Pt-SnS_2 surface is chemisorbed. The TDOS and PDOS of these three gas molecules adsorbed on Pt_2-SnS_2 are shown in Figure 6d−f,d1−f1, respectively. The adsorption of these three gas molecules leads to different decreases in the original TDOS curves of Pt_2-SnS. It can be observed from the PDOS curves that the hybridization of the atomic orbitals inside the CO adsorbate and the energy interval in which the hybridization occurs are roughly similar to the discussed Pt-SnS_2. For CO_2, Pt-5d, C-2p, and O-2p do not overlap significantly, indicating that no mutual hybridization occurs between these orbitals, confirming that no stable chemical bond is formed between CO_2 and Pt. For NO, Pd-5d hybridizes significantly with N-2p in the −10 to −7.5 and 0 to 2.5 eV energy-level interval. Figure 6g−i,g1−i1 shows the TDOS and PDOS of these three gas molecules adsorbed on Pt_3-SnS_2, respectively. For the adsorption of CO_2, there is little overlap between the atomic orbitals, and no significant hybridization between the orbitals. The TDOS curve near the Fermi energy level slightly decreases, and the conductivity of its adsorption system is slightly enhanced. On the contrary, for the adsorption of CO and NO, the orbitals of Pt metal atoms and the atomic orbitals of the gas undergo drastic hybridization in the energy-level region from −10 to −5 eV, leading to a decrease in the TDOS curve near the Fermi energy level. So the conductivity of these two adsorption systems increases.

Molecular orbital analysis is usually used to observe the changes in the electronic properties of the substrate by adsorbed gas molecules. Figure 7 shows the HOMO and LUMO distributions of Pt_n-SnS_2 before and after the adsorption of CO, CO_2, and NO, and the values of E_g, E_{LUMO}, and E_{HOMO} are indicated accordingly in the figure. Figure 7a−d shows the HOMO and LUMO distributions of Pt-SnS_2 and Pt-SnS_2 after adsorption of these three gases. It can be found that the HOMO and LUMO electron cloud distributions do not change much after CO and CO_2 adsorption. However, after NO adsorption, the HOMO electron cloud distribution is mainly distributed around NO and Pt atoms, and the LUMO electron cloud distribution is mainly distributed around SnS_2. The E_g value of the substrate does not change after CO adsorption, indicating that the system conductivity also does not change much, while CO_2 and NO adsorption leads to an increase in the E_g value of the substrate and a decrease in the conductivity of the system. Figure 7e−h shows the HOMO and LUMO distributions before and after the adsorption of CO, CO_2, and NO on Pt_2-SnS_2. The HOMO and LUMO are mainly distributed near the Pt atoms due to the high chemical activity of the Pt atoms. Likewise, NO has the greatest change on the LUMO distribution of the substrate. Meanwhile, CO_2 has the greatest

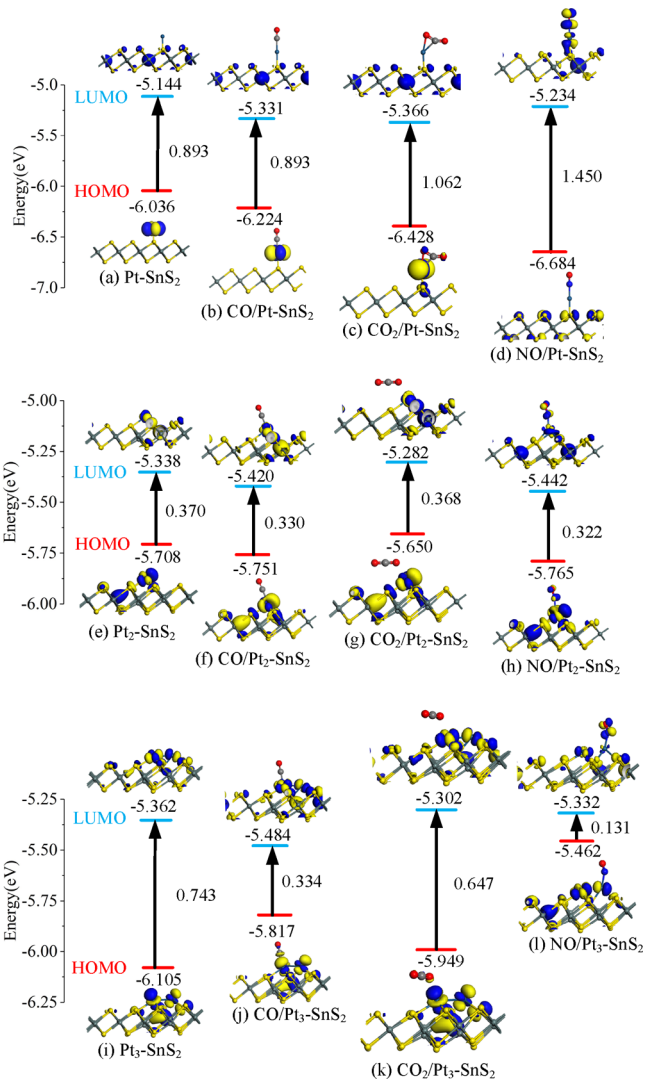

Figure 7. (a−l) HOMO and LUMO of CO, CO_2, and NO adsorption on Pt_n-SnS_2 surfaces.

change on the HOMO distribution of the substrate. The adsorption of CO, CO_2, and NO decreases the E_g value of Pt_2-SnS_2 from 0.370 to 0.330, 0.322, and 0.368 eV, respectively. Figure 7i−l shows the HOMO and LUMO distributions of Pt_3-SnS_2 before and after the adsorption of these three gas molecules. The adsorption of NO has the greatest change on the E_g values of Pt_3-SnS. The E_g value of this system decreased from 0.743 to 0.131 eV. For the adsorption of CO, the E_g value of Pt_3-SnS_2 decreases to 0.334 eV. Similarly, for the adsorption of CO_2, the E_g value decreases and the conductivity of the system increases. The above analysis is consistent with the results of the DOS analysis.

3.4. Adsorption Behavior of CO, CO_2, and NO Gas Molecules on Pt_n-$MoTe_2$. CO, CO_2, and NO are placed on the surface of the Pt_n-$MoTe_2$ monolayer with different angles' proximity, and the structure with the largest absolute value of E_{ads} is selected after geometric optimization to obtain the most stable adsorption structure, as shown in Figure 8. The corresponding adsorption parameters are shown in Table 4. Figure 8a−c shows the most stable structures of CO, CO_2, and NO adsorbed on the Pt-$MoTe_2$ surface. Compared with the intrinsic $MoTe_2$, the adsorption capacity of Pt-$MoTe_2$ is improved for CO, CO_2, and NO, and the corresponding E_{ads}

https://doi.org/10.1021/acsomega.3c04158
ACS Omega 2023, 8, 29746−29757

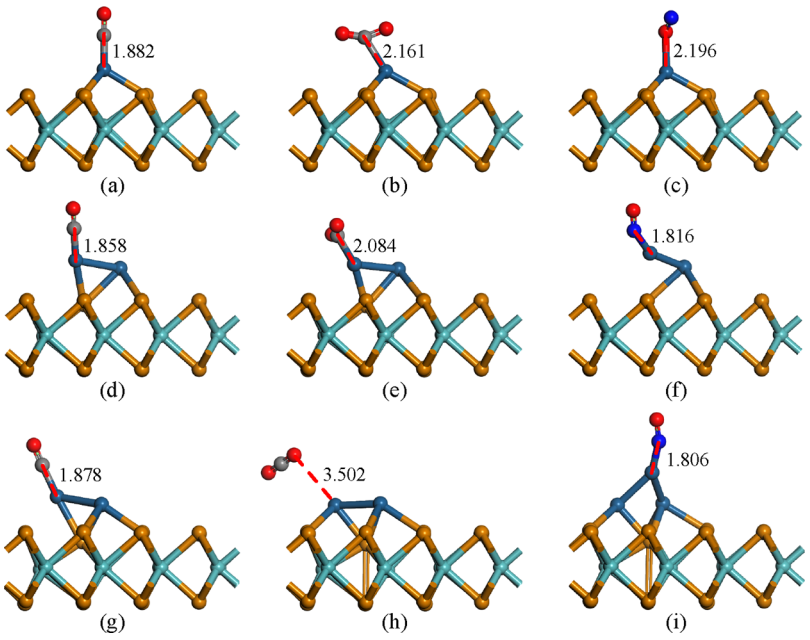

Figure 8. CO, CO_2, and NO adsorption on Pt_n-$MoTe_2$ surfaces. (a–c) Pt-$MoTe_2$; (d–f) Pt_2-$MoTe_2$; (g–i) Pt_3-$MoTe_2$. The distance unit is Å.

Table 4. E_{ads}, Q_t, and Adsorption Distance of Gas Molecules Adsorbed on Pt_n-$MoTe_2$

structure	gas molecules	adsorption distance (Å)	E_{ads} (eV)	Q_t (e)
Pt-$MoTe_2$	CO	1.882	−2.403	−0.0683
	CO_2	2.161	−0.294	−0.2364
	NO	2.196	−0.350	−0.0484
Pt_2-$MoTe_2$	CO	1.858	−2.191	−0.0433
	CO_2	2.084	−0.353	−0.2825
	NO	1.816	−1.938	−0.0389
Pt_3-$MoTe_2$	CO	1.878	−1.950	−0.053
	CO_2	3.502	−0.220	−0.024
	NO	1.806	−2.028	−0.0582

are −2.403, −0.294, and −0.350 eV. At the same time, all three gas molecules form chemical bonds with the surface, and the corresponding adsorption distances are shortened to 1.882, 2.161, and 2.196 Å, respectively. From the Hirshfeld analysis, it can be seen that CO transfers −0.0683 e of electrons to the surface of the substrate, while CO_2 and NO receive electrons from the surface with charges of −0.2364 e and −0.0484 e, respectively, thus indicating that the charge transfer is also enhanced compared to the intrinsic substrate. The most stable structures of the gases adsorbed on the Pt_2-$MoTe_2$ surface are shown in Figure 8d–f. From the structure diagram, it can be found that all of CO, CO_2, and NO form chemical bonds with Pt atoms on the surface, and the corresponding E_{ads} are −2.191, −0.353, and −1.938 eV, and the adsorption distances are 1.858, 2.084, and 1.816 Å, respectively. These adsorption data show an increase in the E_{ads} and a decrease in the adsorption distance of Pt_2-$MoTe_2$ for the gases compared with the adsorption on the intrinsic substrate. In addition, the charge transfer between CO, CO_2, NO and the substrate surface is −0.0433 e, −0.2825 e, and −0.0389 e, respectively. It should be noted that the structure of Pt_2-$MoTe_2$ changed significantly after the adsorption of NO, and this phenomenon is not conducive to the gas desorption process. Finally, Figure 8g–i illustrates the structural models of Pt_3-$MoTe_2$ adsorbed gas molecules. Except for CO_2, both CO and NO form chemical bonds with Pt atoms on the substrate surface. The E_{ads} of CO, CO_2, and NO on the Pt_3-$MoTe_2$ surface are increased to −1.950, −0.220, and −2.028 eV, respectively; meanwhile, the adsorption distances are shortened to 1.878, 3.502, and 1.806 Å, respectively. Except for NO, which gets −0.053 e of electrons, both CO and CO_2 provide electrons to the substrate, and the transferred charges are −0.024 e and −0.0582 e. In addition, it can be found that the structure of Pt_3-$MoTe_2$ is severely deformed after adsorption of NO, so the structure is not suitable for NO detection or adsorption. It is worth mentioning an interaction between CO_2 and Pt in Pt-$MoTe_2$ and Pt_2-$MoTe_2$, yet there appears to be no interaction with Pt_3-$MoTe_3$. This is because for Pt-$MoTe_2$ and Pt_2-$MoTe_2$, the adsorption distance of CO_2 is small, the absolute value of E_{ads} is large, and the charge transfer amount is large, indicating that the interaction is intense, resulting in the formation of a chemical bond between the C atoms of CO_2 and Pt, and the CO_2 also has some deformation. In contrast, the adsorption distance of CO_2 on Pt_3-$MoTe_3$ is far, the absolute value of E_{ads} is small, and the charge transfer is weak, indicating that this interaction is weak, and no chemical bond is formed in the adsorption process.

Figure 9 shows the TDOS and PDOS curves of all adsorption systems based on Pt_n-$MoTe_2$. For the TDOS and PDOS of gas-adsorbed Pt-$MoTe_2$ systems shown in Figure 9a–c,a1–c1, the adsorption of CO and CO_2 on Pt-$MoTe_2$ causes the TDOS curves near the Fermi energy level to increase to different degrees, signifying that the conductivity of these two adsorption systems decreases. However, for NO adsorption, the conductivity of the system increases due to the decrease in the TDOS curve. The hybridization phenomenon of atomic orbitals is responsible for the alteration of TDOS curves, which can be observed by PDOS curves. Pt-5d undergoes orbital hybridization with C-2p and O-2p of CO in the energy-level interval from −7.5 to 1.3 eV. The curve peaks of Pt-5d overlap with C-2p and O-2p of CO_2 near the −8.7, −7.5, −7, −3.8, −0.2, and 1.3 eV energy levels. Meanwhile, for NO, Pt-5d, N-2p, and O-2p in the −9 to 1

https://doi.org/10.1021/acsomega.3c04158
ACS Omega 2023, 8, 29746−29757

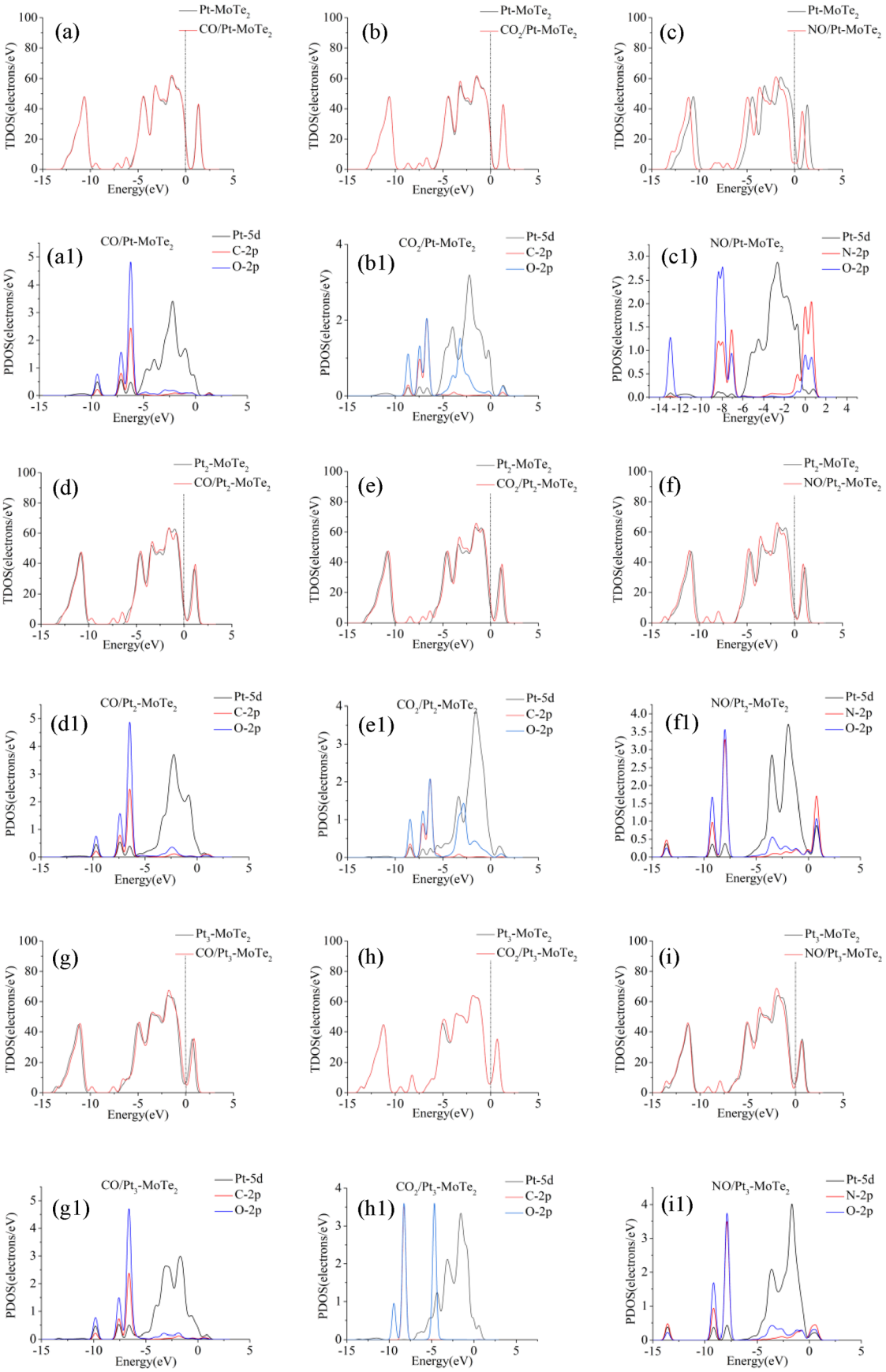

Figure 9. (a–i) TDOS and PDOS of CO, CO_2, and NO adsorption on Pt_n-$MoTe_2$ surfaces.

https://doi.org/10.1021/acsomega.3c04158
ACS Omega 2023, 8, 29746−29757

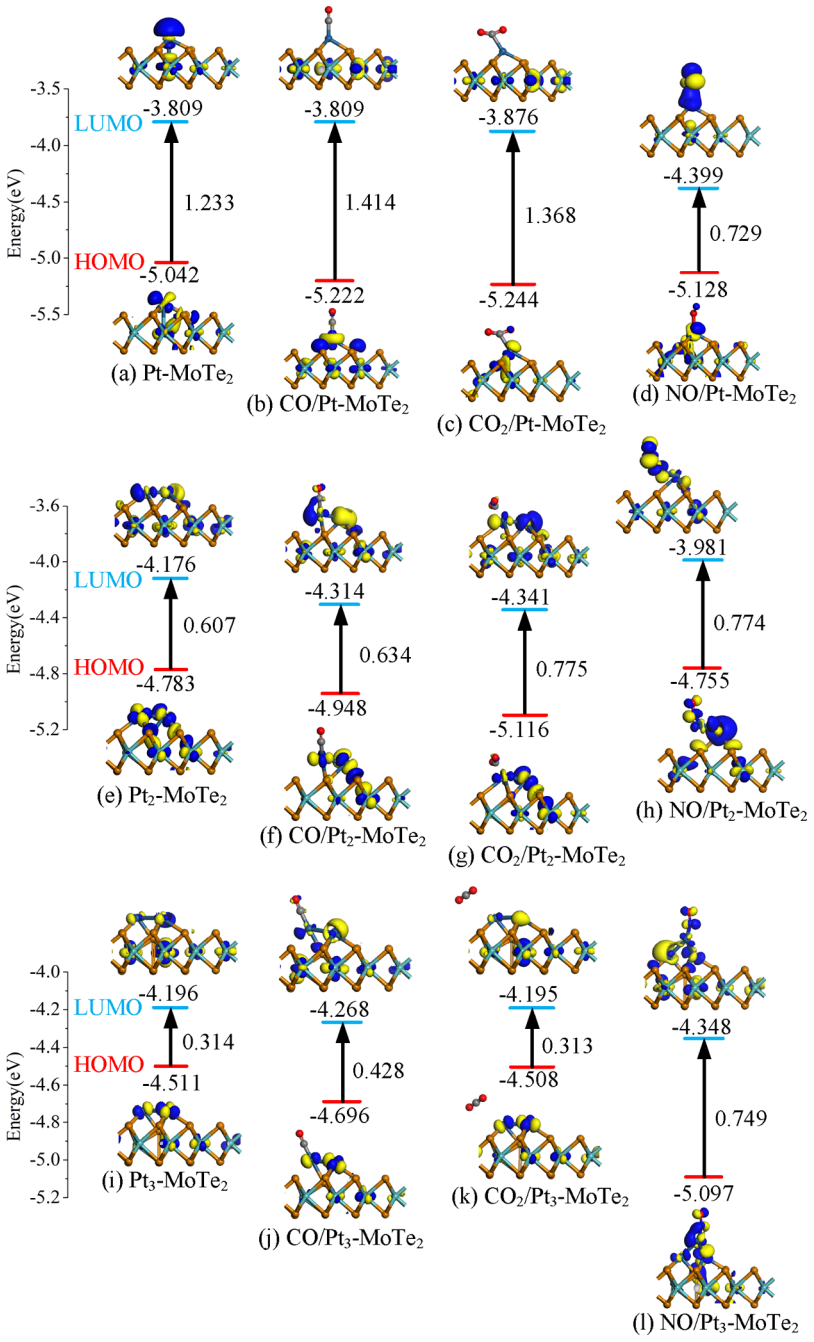

Figure 10. (a–l) HOMO and LUMO of CO, CO_2, and NO adsorption on Pt_n-$MoTe_2$ surfaces.

eV energy-level region undergo a strong orbital hybridization phenomenon. The TDOS and PDOS of these three gas molecules adsorbed on Pt_2-$MoTe_2$ are shown in Figure 9d–f,d1–f1, respectively. The adsorption of the three gas molecules raises the original TDOS curves of Pt_2-$MoTe_2$. As can be observed from the PDOS curves, the hybridization of the atomic orbitals within these three adsorbed bodies and the intervals in which the hybridization occurs are roughly similar to those discussed for Pt-$MoTe_2$. Only for NO, the hybridization of each atomic orbital in the −5 to 1.3 eV energy-level interval is significantly enhanced. Figure 9g–i,g1–i1 shows the TDOS and PDOS of these three gas molecules adsorbed on Pt_3-$MoTe_2$, respectively. For CO_2 adsorption, the conductivity of this adsorption system remains almost constant because the weak hybridization between the atomic orbitals causes almost no change in the TDOS curve near the Fermi energy level. In contrast, for both CO and NO adsorption, the orbitals of Pt metal atoms and the atomic orbitals of the gases undergo drastic hybridization in the −10 to 1.2 eV energy-level region, causing an increase in the TDOS curve near the Fermi energy level.

The change in the electronic properties of adsorption systems was analyzed from the perspective of molecular orbitals. Figure 10 shows the HOMO and LUMO distributions of Pt_n-$MoTe_2$ before and after the adsorption of CO, CO_2, and NO, and the values of E_g, E_{LUMO}, and E_{HOMO} are marked accordingly. The HOMO and LUMO distributions of Pt-$MoTe_2$ and Pt-$MoTe_2$ after adsorption of these three gases are shown in Figure 10a–d. NO has the greatest effect on the LUMO distribution of Pt-$MoTe_2$, with the E_{LUMO} value

https://doi.org/10.1021/acsomega.3c04158
ACS Omega 2023, 8, 29746−29757

changing from the original −3.809 to −4.399 eV. NO adsorption causes the E_g value of the substrate to decrease, while both CO and CO_2 cause the increase of E_g, and correspondingly, the conductivity of the former increases and the latter decreases. Figure 10e−h shows the HOMO and LUMO distributions of Pt_2-$MoTe_2$ before and after gas adsorption. HOMO and LUMO are mainly distributed near Pt atoms due to the strong chemical activity of Pt atoms. Similarly, NO has the greatest effect on the LUMO distribution of the substrate. And CO_2 has the greatest effect on the substrate HOMO distribution. The adsorption of CO, CO_2, and NO increases the E_g values of Pt_2-$MoTe_2$ from 0.607 to 0.634, 0.775, and 0.774 eV, respectively. Figure 10i−l shows the HOMO and LUMO distributions of Pt_3-$MoTe_2$ before and after the adsorption of these three gas molecules. The effect of NO adsorption on the values of E_g, E_{LUMO}, and E_{HOMO} and the HOMO and LUMO distributions of Pt_3-$MoTe_2$ is the greatest. The E_g value for this system increased from 0.314 to 0.749 eV. For CO adsorption, the E_g value of Pt_3-$MoTe_2$ increased to 0.428 eV. In contrast, for CO_2 adsorption, the conductivity did not change significantly due to the almost unchanged E_g value. The above analysis is consistent with the results of the TDOS analysis.

4. CONCLUSIONS

In this study, the intrinsic SnS_2 and $MoTe_2$ and the Pt_n-cluster-doped SnS_2 and $MoTe_2$ were proposed as potential gas-sensitive materials for exploring an effective detection method for the noxious vehicle emission gases: CO, CO_2, and NO. Multi-perspective calculations were performed by analyzing the E_{ads}, adsorption distance, and charge transfer amount as well as TDOS, PDOS, and molecular orbitals. The results show that Pt-cluster doping improves the conductivity of intrinsic SnS_2 and $MoTe_2$. In contrast to the physical adsorption of intrinsic SnS_2 and $MoTe_2$, gas adsorption on Pt_n-SnS_2 is chemisorbed, except for CO_2 adsorption, and the E_{ads} is significantly increased and the adsorption distance is significantly reduced. According to the DOS and molecular orbital analysis, the conductivity of the adsorption system of Pt-SnS_2 remains almost unchanged after the adsorption of CO, so Pt-SnS_2 is not suitable for the detection of CO gases. Pt-SnS_2 maintains good gas-sensitive properties for CO_2 and NO, and Pt_2-SnS_2 maintains good gas-sensitive properties for CO and NO. The adsorption of CO, CO_2, and NO on intrinsic $MoTe_2$ is a weakly interacting physical adsorption. Doping of one to three Pt atoms leads to different degrees of enhancement of the adsorption capacity of the substrates for these three target gases. However, for Pt_2-$MoTe_2$ and Pt_3-$MoTe_2$, the structure of these two materials undergoes significant deformation upon NO adsorption. Based on the DOS and molecular orbital analysis, the interaction between Pt_3-$MoTe_2$ and CO_2 is weak, and the conductivity of this system is almost unaffected by CO_2 adsorption. Generally, Pt_n-$MoTe_2$ (n = 1−3) can realize good gas-sensitive properties for CO, CO_2, and NO. Based on the calculation results, this paper provides a theoretical basis for the development of gas sensors for the detection of vehicle emission gases.

AUTHOR INFORMATION

Corresponding Author

Shoucheng Yan − *College of Energy Engineering, Huanghuai University, Zhumadian 463000, China;* orcid.org/0009-0001-2021-6197; Email: shouchengyanhu@outlook.com

Authors

Yanshan Zhang − *College of Energy Engineering, Huanghuai University, Zhumadian 463000, China;* orcid.org/0000-0002-0383-1323

Yawei Zhu − *Guangdong Creation Acoustic Technology Co., Ltd., Guangzhou 511408, China*

Complete contact information is available at: https://pubs.acs.org/10.1021/acsomega.3c04158

Notes

The authors declare no competing financial interest.

ACKNOWLEDGMENTS

This study was supported by the Programs for Science and Technology Development of Henan Province (nos. 222102240108, 182102110115, and 182102310850).

REFERENCES

(1) Sun, S.; Jin, J.; Xia, M.; Liu, Y.; Gao, M.; Zou, C.; Wang, T.; Lin, Y.; Wu, L.; Mao, H.; Wang, P. Vehicle emissions in a middle-sized city of China: Current status and future trends. *Environ. Int.* **2020**, *137*, No. 105514.

(2) Kampa, M.; Castanas, E. Human health effects of air pollution. *Environ. Pollut.* **2008**, *151*, 362−367.

(3) Akitt, J. W. Some observations on the greenhouse effect at the Earth's surface. *Spectrochim. Acta, Part A* **2018**, *188*, 127−134.

(4) Burns, D. A.; Aherne, J.; Gay, D. A.; Lehmann, C. M. B. Acid rain and its environmental effects: Recent scientific advances. *Atmos. Environ.* **2016**, *146*, 1−4.

(5) Verma, R.; Vinoda, K. S.; Papireddy, M.; Gowda, A. N. S. Toxic pollutants from plastic waste-a review. *Procedia Environ. Sci.* **2016**, *35*, 701−708.

(6) Wang, M.; Cheng, S.; Zeng, W.; Zhou, Q. Adsorption of toxic and harmful gas CO on TM (Ni, Pd, Pt) doped $MoTe_2$ monolayer: A DFT study. *Surf. Interfaces* **2022**, *31*, No. 102111.

(7) Xia, S.-Y.; Tao, L.-Q.; Jiang, T.; Sun, H.; Li, J. Rh-doped h-BN monolayer as a high sensitivity SF_6 decomposed gases sensor: A DFT study. *Appl. Surf. Sci.* **2021**, *536*, No. 147965.

(8) Lu, X.; Guo, L.; Wang, P.; Cui, M.; Kanghong, D.; Peng, W. RETRACTED: Theoretical investigation of the adsorption of gas molecules on WSe2 monolayers decorated with Pt, Au nanoclusters. *Appl. Surf. Sci.* **2020**, *513*, No. 145860.

(9) Gui, Y.; Luo, P.; Ji, C.; Lin, Y.; Chen, X. First-Principles Study of the Gas Sensing of Benzene and Formaldehyde by Ag_2O- and CuO-Modified $MoSe_2$ Nanosheets. *ACS Appl. Nano Mater.* **2022**, *5*, 12907−12914.

(10) A., Zhang; A., Dong; Y., Gui Gas-Sensing Properties of B/N-Modified SnS_2 Monolayer to Greenhouse Gases (NH_3, Cl_2, and C_2H_2), in: *Materials*, 2022, DOI: 10.3390/ma15155152.

(11) Gong, W.; Liu, J.; Gui, Y.; Huang, H. Adsorption of Greenhouse Decomposition Products on Ag2O−SnS2 and CuO−SnS2 Surfaces. *ACS Omega* **2022**, *7*, 21043−21051.

(12) Ngo, H. M.; Pal, U.; Kang, Y. S.; Ok, K. M. DFT-Based Study for the Enhancement of CO_2 Adsorption on Metal-Doped Nitrogen-Enriched Polytriazines. *ACS Omega* **2023**, *8*, 8876−8884.

(13) Yao, X.; Wang, Y.; Lang, X.; Zhu, Y.; Jiang, Q. Thickness-dependent bandgap of transition metal dichalcogenides dominated by interlayer Van der Waals interaction. *Phys. E* **2019**, *109*, 11−16.

(14) Yao, X.; Wang, Y.-R.; Lang, X.-Y.; Zhu, Y.-F.; Jiang, Q. Composition- and layer-dependent bandgap of two-dimensional transition metal dichalcogenides alloys. *Phys. E* **2020**, *124*, No. 114243.

(15) Yao, X.; Chen, Z.; Wang, Y.; Lang, X.; Gao, W.; Zhu, Y.; Jiang, Q. Activated basal planes of WS_2 by intrinsic defects as catalysts for the electrocatalytic nitrogen reduction reaction. *J. Mater. Chem. A* **2019**, *7*, 25961−25968.

(16) Yao, X.; Chen, Z.-W.; Liu, G.-J.; Lang, X.-Y.; Zhu, Y.-F.; Gao, W.; Jiang, Q. Steric Hindrance- and Work Function-Promoted High Performance for Electrochemical CO Methanation on Antisite Defects of MoS_2 and WS_2. *ChemSusChem* **2021**, *14*, 2255−2261.
(17) Chen, Y.; Gui, Y.; Chen, X. Adsorption and gas-sensing properties of C_2H_4, CH_4, H_2, H_2O on metal oxides (CuO, NiO) modified SnS_2 monolayer: A DFT study. *Results Phys.* **2021**, *28*, No. 104680.
(18) Peng, R.; Zeng, W.; Zhou, Q. Adsorption and gas sensing of dissolved gases in transformer oil onto Ru_3-modified SnS_2: A DFT study. *Appl. Surf. Sci.* **2023**, *615*, No. 156445.
(19) Shi, Z.; Zhang, J.; Zeng, W.; Zhou, Q. Adsorption and Sensing Performances of $MoTe_2$ Monolayers Doped with Pd, Ni, and Pt for SO_2 and NH_3: A DFT Investigation. *Langmuir* **2023**, *39*, 4125−4139.
(20) Liu, Y.; Ren, M.; Song, B.; Dong, M. A DFT study of toxic gases (NH_3, C_2H_2, NO) adsorption and detection on metal oxides (CuO, Ag_2O, In_2O_3) modified $MoTe_2$ monolayer. *Appl. Surf. Sci.* **2023**, *622*, No. 156858.
(21) Jiang, T.; Zhang, W.; Zhang, T.; Yuan, H.; Bi, M.; Zhou, X. Adsorption and gas-sensing performances of C_2H_2, C_2H_4, CO, H_2 in transformer oil on Pt-doped $MoTe_2$ monolayer: A DFT study. *Phys. E* **2023**, *146*, No. 115568.
(22) Chen, J.; Zhou, Q.; Jia, L.; Cui, X.; Zeng, W. The gas-sensing mechanism of Pt_3 cluster doped SnS_2 monolayer for SF_6 decomposition: A DFT study. *Appl. Surf. Sci.* **2022**, *597*, No. 153693.
(23) A., Zhang; Q., Dong; Y., Gui; J., Li; F., Wan Gas-Sensing Property of TM-$MoTe_2$ Monolayer towards SO_2, SOF_2, and HF Gases, in: *Molecules*, 2022, DOI: 10.3390/molecules27103176.
(24) Gui, Y.; Yang, S.; Ji, C.; Chen, X. Adsorption properties of Ni cluster modified TiO_2 (1 0 1) towards SF_6 decomposition gases. *High Voltage* **2023**, *8*, 158−170.
(25) Liu, Z.; Gui, Y.; Xu, L.; Chen, X. Adsorption and gas-sensing properties of Au_n (n = 1−3) cluster doped $MoTe_2$ for NH_3, NO_2, and SO_2 gas molecules. *Surf. Interfaces* **2022**, *30*, No. 101883.
(26) Hu, X.; Gui, Y.; Zhu, S.; Chen, X. Transition metal oxides (NiO, SnO_2, In_2O3) modified graphene: A promising candidate to detect and scavenge CO, C_2H_2, and CH_4 gases. *Diamond Relat. Mater.* **2022**, *123*, No. 108856.
(27) Zhou, R.; Wu, S.; Cui, H.; Li, P.; Wu, T. First-principles investigation of Pt-doped $MoTe_2$ for detecting characteristic air decomposition components in air insulation switchgear. *Comput. Theor. Chem.* **2022**, *1214*, No. 113796.
(28) Gui, Y.; Hu, X.; Zhu, S.; Chen, X. A DFT study of transition metal (Ag, Au, Co) modified SnS_2 monolayer for the detection and adsorption of the representative gases (NH_3, Cl_2, and C_2H_2) in greenhouses. *Mater. Today Commun.* **2022**, *33*, No. 104618.
(29) Chen, Y.; Gui, Y.; Ding, Z.; Xu, L.; Chen, X. Adsorption and gas-sensing properties of Pd_n-GaNNTs to C_2H_2 and H_2 gases. *Phys. E* **2022**, *136*, No. 115004.
(30) Zhang, Q.; Gui, Y.; Qiao, H.; Chen, X.; Cao, L. Theoretical study of SF_6 decomposition products adsorption on metal oxide cluster-modified single-layer graphene. *J. Ind. Eng. Chem.* **2022**, *105*, 278−290.
(31) Liu, Y.; Gui, Y.; Chen, X. Adsorption and sensing performances of ZnO-g-C_3N_4 monolayer toward SF_6 decomposition products. *Phys. E* **2021**, *134*, No. 114909.
(32) Gui, Y.; Liu, Z.; Ji, C.; Xu, L.; Chen, X. Adsorption behavior of metal oxides (CuO, NiO, Ag_2O) modified GeSe monolayer towards dissolved gases (CO, CH_4, C_2H_2, C_2H_4) in transformer oil. *J. Ind. Eng. Chem.* **2022**, *112*, 134−145.

https://doi.org/10.1021/acsomega.3c04158
ACS Omega 2023, 8, 29746−29757